

1 **Estimating the depth and evolution of intrusions at resurgent** 2 **calderas: Los Humeros (Mexico)**

3 Stefano Urbani¹, Guido Giordano^{1,2}, Federico Lucci¹, Federico Rossetti¹, Valerio Acocella¹,
4 Gerardo Carrasco- Núñez³

5 ¹Dipartimento di Scienze, Università degli Studi Roma Tre, L.go S.L. Murialdo 1, I-00146 Rome, Italy

6 ²CNR - IDPA c/o Università degli Studi di Milano, Via Luigi Mangiagalli, 34, 20133 Milano

7 ³Centro de Geociencias, Universidad Nacional Autónoma de México, Campus UNAM Juriquilla, 76100, Queretaro,
8 Mexico

9 *Correspondence to:* Stefano Urbani (stefano.urban@uniroma3.it)

10 **Abstract.** Resurgent calderas are excellent targets for geothermal exploration, as they are associated with the shallow
11 emplacement of magma, resulting in widespread and long lasting hydrothermal activity. Resurgence is classically
12 attributed to the uplift of a block or dome resulting from the inflation of the collapse-forming magma chamber due to
13 the intrusion of new magma. The Los Humeros volcanic complex (LHVC; Mexico), consists of two nested calderas: the
14 outer and older Los Humeros formed at 164 ka and the inner, Los Potreros, formed at 69 ka. The latter is resurgent and
15 currently the site of an active and exploited geothermal field (63 MWe installed). Here we aim at better defining the
16 characteristics of the resurgence in Los Potreros, by integrating field work with analogue models, evaluating the spatio-
17 temporal evolution of the deformation and the depth and extent of the intrusions responsible for the resurgence which
18 may also represent the local heat source(s).

19 Structural field analysis and geological mapping show that the floor of the Los Potreros caldera is characterized by
20 several lava domes and cryptodomes (with normal faulting at the top) that suggest multiple deformation sources
21 localized in narrow areas.

22 Analogue experiments are then used to define the possible source of intrusion responsible for the observed surface
23 deformation. We apply a tested relationship between the surface deformation structures and depth of elliptical sources to
24 our experiments with sub-circular sources. We found that this relationship is independent of the source and surface
25 dome eccentricity and suggest that the magmatic sources inducing the deformation in Los Potreros are located at very
26 shallow depths (hundreds of meters), which is in agreement with the well data and field observations. We propose that
27 the recent deformation at LHVC is not a classical resurgence associated with the bulk inflation of a deep magma
28 reservoir; rather it is related to the ascent of multiple magma bodies at shallow crustal conditions (< 1 km depth). A
29 similar multiple source model of the subsurface structure has been also proposed for other calderas with an active
30 geothermal system (Usu volcano, Japan) suggesting that the model proposed may have wider applicability.

31 **1 Introduction**

32 Caldera resurgence consists of the post-collapse uplift of part of the caldera floor. Resurgence has been described in
33 several calderas worldwide (Smith and Bailey, 1968; Elston, 1984; Lipman, 1984 and references therein), representing a
34 frequent step in caldera evolution. Several mechanisms that trigger resurgence have been invoked, including the
35 pressurization of the hydrothermal system (Moretti et al., 2018), regional earthquakes (Walter et al., 2009), and
36 magmatic intrusion (Kennedy et al. 2012). Discriminating the contributions to the observed uplift of each of these
37 mechanisms is often challenging (Acocella, 2014). However, despite the possible hydrothermal and tectonic
38 contributions, field observations in eroded resurgent calderas (e.g. Tomochic, Swanson and McDowell, 1985; Kutcharo,

39 Goto and McPhie 2018; Turkey Creek, Du Bray and Pallister, 1999) coupled with the long timescale of the uplift of the
40 caldera floor (from tens to thousands of years), suggest that the intrusion of magmatic bodies is the prevalent
41 mechanism for resurgence.

42 Resurgence is commonly attributed to the emplacement of silicic magmas at different depth levels under limited
43 viscosity contrasts with regard to the previously emplaced magma (Marsh, 1984; Galetto et al., 2017). However, though
44 rare, resurgence may be also triggered by the injection of more primitive magma (Morán-Zenteno et al., 2004; Kennedy
45 et al., 2012) or by the emplacement of basaltic sills, as recently documented at the Alcedo caldera (Galapagos; Galetto
46 et al., 2019). The shape of the intracaldera resurgent structures is variable, being characterized by elliptical domes with
47 longitudinal graben(s) at the top (e.g. Toba; De Silva et al., 2015; Snowdonia, Beavon, 1980; Timber Mountain,
48 Christiansen et al., 1977) or, less commonly, by sub-circular domes (e.g. Cerro Galan, Folkes et al., 2011; Long Valley,
49 Hildreth et al., 2017; Grizzly Peak, Fridrich et al., 1991) with both longitudinal grabens (Long Valley) or concentric
50 fault blocks (Grizzly Peak) at their top.

51 Whatever is the shape, resurgence is often associated with hydrothermal and ore forming processes, since the circulation
52 pattern and temperature gradients of geothermal fluids are structurally-controlled by the space-time distribution of faults
53 and fractures and by the depth and shape of the magmatic sources (e.g. Guillou Frottier et al., 2000; Prinbow et al.,
54 2003; Stix et al., 2003; Mueller et al., 2009; Giordano et al., 2014; Kennedy et al., 2018). Therefore, the characterisation
55 of the magma that drives resurgence (location, depth and size) and of the factors controlling the release of heat
56 (permeability, fracture patterns, and fluid flow) have important implications for the exploration and exploitation of
57 renewable geothermal energy resources. In particular, the estimation of the location, depth and geometry of the
58 magmatic sources is crucial to define the geothermal and mineral potential of resurgent calderas, allowing an
59 economically sustainable exploration and exploitation of their resulted natural resources.

60 The depth and size of the magmatic sources influence the deformation style of the resurgence at the surface (Acocella et
61 al., 2001). Deep sources (i.e. depth/diameter ratio ~ 1 assuming a spherical source) are associated with resurgent blocks
62 (e.g. Ischia and Pantelleria, Acocella and Funicciello, 1999; Catalano et al., 2009), whereas shallower sources (i.e.
63 depth/diameter ratio ~ 0.4) to resurgent domes (e.g. Valles and Yenkahe, Kennedy et al., 2012; Brothelande et al., 2016).
64 Moreover, uplift rates may change by one order of magnitude from ~ 1 to ~ 10 cm per year (e.g. Yellowstone and Iwo
65 Jima, Chang et al., 2007; Ueda et al., 2018). Nevertheless, despite showing different uplift styles and rates, these natural
66 examples share a common feature that is a coherent uplift of the caldera floor. A different style of deformation is
67 observed at calderas characterized by the widespread and delocalized uplift of several minor portions of the caldera
68 floor, associated with the shallow emplacement of sills and cryptodomes, as observed at Usu volcano (Japan,
69 Matsumoto and Nakagawa, 2010; Tomya et al., 2010). Such deformation pattern suggests different depth(s) and
70 extent(s) of the magma source(s). A better assessment of the subsurface structure in this type of calderas has crucial
71 implications for geothermal exploration.

72 The Los Humeros Volcanic Complex (LHVC, Mexico) is an important geothermal target area, consisting of two nested
73 calderas: Los Humeros (the outer, larger and older one; 164 ka) and Los Potreros (the inner, smaller and younger one;
74 69 ka) (Fig. 1). The latter is characterized by the resurgence of its floor, interpreted to be due to the inflation of the
75 magma chamber responsible for the collapse, with its top at ca 5 km depth (Norini et al., 2015, 2019).

76 This paper aims to (1) evaluate the depth of the intrusion(s) inducing the uplift in the LHVC area; (2) explain the spatio-
77 temporal evolution of the observed deformation of the caldera floor; and (3) test the validity of the linear relationship
78 between the surface deformation structures and depth of elliptical sources (Brothelande and Merle 2015) for sub-
79 circular sources. To achieve these goals, we integrate results from structural field investigations carried out within the

80 Los Potreros caldera with those derived from analogue experiments specifically designed to constrain the depth of the
81 deformation source(s) in volcanic caldera environments. The obtained results show that: (1) the relation between the
82 source depth and surface deformation structures is independent of the source eccentricity; (2) the LHVC is
83 characterized by discontinuous and small-scale (areal extent $\sim 1 \text{ km}^2$) surface deformations generated from multiple and
84 shallow-emplaced ($< 1 \text{ km}$ depth) magmatic bodies. These results should be taken into account for the planning of
85 future geothermal operations at the LHVC and in other calderas showing similar surface deformation.

86 **2 Geological-structural setting**

87 LHVC is located at the eastern termination of the Trans Mexican Volcanic Belt (TMVB, see inset in Fig. 1). The TMVB
88 is the largest Neogene volcanic arc in Mexico ($\sim 1000 \text{ km}$ long and up to $\sim 300 \text{ km}$ wide), commonly associated with the
89 subduction of the Cocos and Rivera plates beneath the North American plate along the Middle American trench (Ferrari
90 et al., 2012, and references therein). The LHVC consists of two nested calderas formed during the Pleistocene: the outer
91 $18 \times 16 \text{ km}$ Los Humeros caldera and the inner $10 \times 8 \text{ km}$ Los Potreros caldera (Fig. 1, Ferriz and Mahood, 1984;
92 Norini et al., 2015; Carrasco-Núñez et al., 2017b).

93 Based on updated stratigraphic and geochronological information, the evolution of the LHVC can be divided into three
94 main eruptive stages (Table 1, Carrasco-Núñez et al., 2017b, 2018). Pre-caldera volcanism extended between ca. 700
95 and 164 ka (zircon U-Th and feldspar $^{39}\text{Ar}/^{40}\text{Ar}$ ages, Carrasco-Núñez et al., 2018), showing evidence for an extended
96 building phase leading to the establishment of the large volume rhyolitic reservoir, which fed several lava domes
97 erupted to the western border of the Los Humeros Caldera. A Caldera stage started at ca. 164 ka (zircon U-Th and
98 feldspar $^{39}\text{Ar}/^{40}\text{Ar}$ ages, Carrasco-Núñez et al., 2018), with the eruption of the $>115 \text{ km}^3$ (dense rock equivalent volume)
99 Xaltipan ignimbrite that triggered the collapse of the Los Humeros caldera. This was followed by a Plinian eruptive
100 episodic sequence, characterized by the emplacement of several rhyodacitic pumice fallout layers grouped as the Faby
101 Tuff (Ferriz and Mahood, 1984). The Caldera stage ended with the eruption of the 15 km^3 (dense rock equivalent
102 volume) Zaragoza rhyodacite-andesite ignimbrite at $69 \pm 16 \text{ ka}$ (feldspar $^{39}\text{Ar}/^{40}\text{Ar}$ ages, Carrasco-Núñez et al., 2018)
103 associated with the collapse of the nested Los Potreros caldera.

104 A post-caldera stage ($< 69 \text{ ka}$) is interpreted by Carrasco-Núñez et al. (2018) as composed by two main eruptive phases:
105 (i) a late Pleistocene resurgent phase, characterized by the emplacement of silica-rich small domes and disperse
106 explosive activity within Los Potreros caldera, followed by (ii) Holocene basaltic to trachytic monogenetic volcanism
107 both inside and at the caldera-rim. This eruptive behaviour indicates a change in the configuration of the magmatic
108 plumbing system compared to the caldera stage of Los Humeros, when a single, large and homogenized magma
109 reservoir was in existence (e.g. Ferriz and Mohood, 1984; Verma, 1985). Volcanological and petrological data indicate
110 that the post-caldera volcanism is associated with a heterogeneous multi-layered system vertically distributed within the
111 crust, with a deep (ca. 30 km depth) basaltic reservoir feeding progressively shallower and smaller distinct stagnation
112 layers, pockets and batches up to very shallow conditions (ca. 3km) (Lucci et al., 2020), in agreement with recent
113 conceptual models for magma reservoirs under caldera systems (e.g. Cashman and Giordano, 2014).

114 During the early resurgent phase of the post-caldera stage, rhyolitic domes were emplaced along the northern rim and
115 within the Los Humeros caldera. Available ages span between $44.8 \pm 1.7 \text{ ka}$ (zircon U-Th dating) and $50.7 \pm 4.4 \text{ ka}$
116 (feldspar $^{39}\text{Ar}/^{40}\text{Ar}$ dating, Carrasco-Núñez et al., 2018). This effusive activity was followed by several explosive
117 eruptions, which originated a dacitic air fall called Xoxoctic Tuff (0.6 km^3 , Ferriz and Mahood, 1984) and a pyroclastic
118 sequence that includes an explosive breccia and pyroclastic flow deposits comprising the Llano Tuff (Ferriz and
119 Mahood 1984; Willcox, 2011).

120 The Holocene ring-fractures fed bimodal magmatism characterized by both explosive and effusive activity, producing
121 several lava flows and domes, as well as the ca. 7 ka (C-14 age, Dávila-Harris and Carrasco-Núñez, 2014) Cuicuiltic
122 Member during periods of dominant explosive activity. The Cuicuiltic Member consists of alternating pumices and
123 scoriae erupted during contemporaneous sub-Plinian to Strombolian activity from multiple vents located mostly along
124 the inner part of the caldera and outer caldera ring faults (Dávila-Harris and Carrasco-Núñez, 2014). During this phase,
125 less evolved lavas (trachyandesite to basalt) were erupted within and outside the Los Potreros caldera, including the
126 olivine-bearing basaltic lava that fills the previously formed Xalapasco crater (Fig. 1). Trachytic lava flows are the most
127 recent products in the area, with an age of ca. 2.8 ka (C-14 age, Carrasco-Núñez et al., 2017b).

128 The reconstruction of the shallow stratigraphy within the Los Potreros caldera is chiefly derived from the analysis of
129 available well-logs (Figs. 2a-b Carrasco-Núñez et al., 2017a, b). Overall, the post-caldera units are lithologically
130 dominated by lava flows resting on ignimbrite deposits emplaced during the caldera stage. Ignimbrites of the caldera
131 stage rest in turn on a thick sequence dominated by andesite lavas dated at ca. 1.4-2.8 Ma (feldspar $^{39}\text{Ar}/^{40}\text{Ar}$ dating,
132 Carrasco-Núñez et al., 2017a). The subsurface geometry of the pre- and syn-caldera products is shown in Figs. 2a-b,
133 where the in-depth geometry of the different magmatic products is cross-correlated and projected along the N-S and E-
134 W direction, respectively. The N-S projection shows a constant depth of the top surface of the pre-caldera andesites that
135 is associated with a highly variable depth (down to -400 m) of the top surface of the syn-caldera Xaltipan ignimbrite.
136 The W-E projection shows a higher depth variability of both the top surface of the pre-caldera group (down to -500 m
137 between H-19 and H-25 wells) and that of the Xaltipan ignimbrite (down to -400 m between H-19 and H-10 wells).
138 Basaltic and rhyolitic-dacitic lavas occur at various depths (Carrasco-Núñez et al., 2017a); rhyolites-dacites are located
139 mostly at the base (H-20 and H-26 wells) or within (H-05 well) the caldera group or the old andesite sequence (H-25
140 and H-19 wells). Basalts are located only within the pre-caldera andesite sequence, both at its base (in contact with the
141 limestone basement; H-5 and H-8 wells) and at its top (in contact with the base of the caldera sequence; H-10 well).
142 These bimodal lava products, showing an irregular lateral distribution, have been interpreted as subaerial (Carrasco-
143 Núñez et al., 2017a).

144 The structural architecture of the LHVC is controlled by a network of active extensional fault systems, made of NNW-
145 SSE, N-S, NE-SW and E-W striking fault strands cutting across the Los Potreros caldera floor. The following main
146 faults were recognised (Norini et al., 2015, 2019; Calcagno et al., 2018) (Fig.1): (i) Maxtaloya (NNW-SSE striking), (ii)
147 Los Humeros and Loma Blanca (N-S striking), (iii) Arroyo Grande (NE-SW striking), (iv) Las Viboras and Las Papas
148 (E-W striking). Such active fault systems are interpreted as due to the recent/active resurgence of the Los Potreros
149 Caldera. Since the faults do not show continuity beyond the caldera border, their scarps decrease in height towards the
150 periphery of the caldera and the dip-slip displacement vectors show a semi-radial pattern (Norini et al., 2015).

151 The source of the areal uplift has been inferred to be the inflation of a saucer or cup shaped deep magmatic source
152 elongated NNW-SSE, up warping a 8 x 4 km resurgent block, centred in the SE portion of the caldera, delimited to the
153 W by the NNW-SSE main faults, and toward the north, east and south by the caldera rim (Fig.1, Norini et al., 2015,
154 2019).

155 The seismic activity between 1994-2017 is clustered along the Loma Blanca, Los Humeros and Arroyo Grande faults
156 (Lermo et al., 2018; Fig. 1). Most of the earthquakes show a magnitude (M_w) between 1 and 2.5 and have been mainly
157 interpreted as induced by the geothermal exploitation activity (injection of fluids and hydrofracturing; Lermo et al.,
158 2018). Four major earthquakes (M_w = 3.2, 3.6, 3.9 and 4.2, at a depth of 1, 4, 2.2 and 1.8 km, respectively) have also
159 been reported, with focal depths close to the trace of the active faults (Loma Blanca and Los Humeros, Fig.1). Such

160 major earthquakes have been interpreted as triggered by fault reactivation due to fluid/brine circulation injected from
161 geothermal wells (Lermo et al., 2018).

162 **3 Methods**

163 This study is based on structural field work combined with analogue models aimed at constraining the depth of the
164 deformation sources in the caldera domain. We also tested if the relation that constrains the depth of the source
165 deformation from surface parameters adopting elliptical sources (Brothelande and Merle 2015) is verified also for sub-
166 circular sources.

167 **3.1 Structural field work**

168 Structural field work was carried out on the post-caldera (Late Pleistocene to Holocene) deposits to characterise the
169 surface deformation related to the recent activity of the Los Potreros caldera and constrain the morphotectonic
170 fingerprints of the resurgence to evaluate its source and areal extent. The geometry and distribution of the observable
171 faults and joints were defined at the outcrop scale by measuring their attitudes (strike and dip; right-hand rule) and
172 spacing. Fault kinematics was assessed through classical criteria on slickensides fault surfaces, such as Riedel shears,
173 growth fibres and sheltering trails (Doblas, 1998). The published geological map (Carrasco-Núñez et al., 2017b) and
174 geothermal well data have been used (Carrasco-Núñez et al., 2017a) to correlate the surface structures at a broader
175 scale. The relationships between faulting and alteration have been assessed (e.g. Giordano et al. 2013; Vignaroli et al.
176 2013, 2015).

177 **3.2 Analogue models: experimental set-up and scaling**

178 Five experiments were undertaken to simulate the ascent of a viscous sub-circular intrusion in a brittle overburden to
179 test the validity of existing relationships between the depth of elliptical intrusions and the observed surface deformation
180 (Brothelande and Merle, 2015). The experimental set-up (Fig. 3) consists of a 31 × 31 cm glass box filled with a sand
181 pack (crust analogue) of variable thickness (T , of 10, 30 and 50 mm, respectively). In each experiment we imposed a
182 layering using a non-cohesive marine sand below a layer of crushed silica sand (grain size = 40-200 μm , cohesion = 300
183 Pa), fixing the thickness ratio of the two layers (T_u/T_l) to 1, to simulate the stratigraphy in Los Potreros (stiffer post
184 caldera lava flows above softer and less cohesive ignimbrite deposits emplaced during the caldera collapse stage). At
185 the base of the sand pack, a piston, controlled by a motor, pushes upward the silicone (magma analogue) placed inside a
186 cylinder 8 cm in diameter. The injection rate is fixed for all the experiments to 2 mm/hr and each experiment was
187 stopped at the onset of the silicone extrusion. Both sand and silicone physical properties are listed in Table 2.

188 At the end of each experiment, the surface has been covered with sand to preserve their final topography and was
189 wetted with water for cutting in sections to appreciate the subsurface deformation. Such sections were used to measure
190 the mean dip of the apical depression faults (θ) induced by the rising silicone. A digital camera monitored the top view
191 deformation of each experiment at 0.02 fps and a laser scanner, placed next to the camera, provided high-resolution data
192 (maximum error ± 0.5 mm) of the vertical displacement to measure in detail the geometrical features of the deformation
193 i.e. dome diameter (L_d), apical depression width (L_g) and dome flank mean dip (α). According to the Buckingham-II
194 theorem (Merle and Borgia 1996 and references therein), our models need 7 independent dimensionless numbers to be
195 properly scaled (i.e. 10 variables minus three dimensions; Table 2). Such dimensionless numbers can be defined as the
196 ratios (Π) listed in Table 3. Some values of Π_5 , representing the ratio between the inertial and viscous forces, are very
197

198 small both in nature and experiments (1.3×10^{-20} and 6.1×10^{-10} , respectively), indicating that the inertial forces are
199 negligible compared to the viscous forces in both cases.

200 **4 Results**

201 **4.1 Structural geology**

202 The outcropping post-caldera lithologies within the Los Potreros Caldera consist of: (1) the Cuicuiltic Member, which
203 blankets most of the surface of the upper half of the studied area; (2) basaltic lava flows filling the Xalapasco crater and
204 the NW portion of the caldera; and (3) trachyandesitic and trachytic lava domes and thick flows extending in the
205 southern half of the caldera and rhyolitic domes in its central part (Fig. 4). Field work documented that the more
206 evolved lavas form five nearly N-S trending elliptical domes, distributed in both sides of the Los Humeros Fault (Figs. 4
207 and 5a): (i) a 2 km long \times 1.2 km wide trachytic dome located to the west of the Maxtaloya and Los Humeros faults, (ii)
208 a 1 \times 0.7 km trachyandesitic dome located in a northeast area of the Maxtaloya fault, and (iii) one trachyandesitic and
209 two obsidian smaller domes (0.4 \times 0.2 km) to the eastern side of the Los Humeros Fault (LH-11 in Fig. 4).

210 Field work concentrated on the three main uplifted areas corresponding to the surface expression of the Loma Blanca,
211 Arroyo Grande and Los Humeros faults (labelled LH1-2, LH9 and LH10 respectively in Fig. 4). The observed
212 structures in these uplifted areas (joints and faults) affect the deposits of the post-caldera phase. Based on field
213 evidence, we also propose a revised interpretation of the surface structures identified by previous studies (Norini et al.,
214 2015, 2019), distinguishing between lineaments (morphological linear scarps, with no measurable fault offsets and/or
215 alteration at the outcrop scale), active and inactive faults, instead associated with measurable fault offsets and with
216 active or fossil alteration, respectively (Fig. 4). We detail below the main structures mapped in the studied area,
217 highlighting their temporal and spatial relationships with the post-caldera geological formations. We identified two
218 inactive faults (Maxtaloya and Arroyo Grande), a morphological lineament (Las Papas) and two currently active faults
219 (Los Humeros and Loma Blanca).

220 **4.1.1 Las Papas lineament (sites LH-07, LH-08)**

221 The E-W trending Las Papas lineament is localised within the Cuicuiltic Member (LH-07; Fig. 5b). We identified an
222 erosional surface along the scarp, where unaltered and undeformed Cuicuiltic Member rocks rest above the Xoxotic
223 Tuff (LH-08, Fig. 5c). The E-W trending morphological lineament of Las Papas is probably due to differential erosion
224 of the softer layers of the pyroclastic deposits, successively blanketed by the Cuicuiltic Member.

225 **4.1.2 Arroyo Grande (site LH-09) and Maxtaloya scarps**

226 The NE-SW Arroyo Grande scarp (Fig. 6a) exposes strongly altered and faulted (NW striking faults, mean attitude
227 N144°/68°, number of data (n) = 8) lavas and ignimbrites unconformably covered by the unaltered Cuicuiltic Member
228 (Fig.6b). The offset observed at the outcrop-scale for the single fault strands is ca. 0.5 m, with a dominant normal dip-
229 slip kinematics (pitch angle of the slickenlines ranging 99°-106°). The inferred cumulative displacement at Arroyo
230 Grande is \sim 10 m. Similarly, an outcrop on the Maxtaloya scarp (in front of well H-6) shows altered trachyandesites
231 covered by unaltered Cuicuiltic Member rocks (Fig. 6c).

232 **4.1.3 Los Humeros (site LH-10)**

233 The fault scarp of the N-S striking (mean attitude $N174^{\circ}/73^{\circ}$, $n=8$) Los Humeros Fault exposes the altered portions of
234 the Cuicuiltic Member. Fault population analysis reveals a dominant normal dip-slip (mean pitch angle of the
235 slickenlines: 84°) kinematics, as documented by both Riedel shears and carbonate-quartz growth steps. The main fault
236 surface is sutured by a trachyandesitic extrusion (Fig. 6d), localised along an aligned N-S dome (site LH-11 in Fig. 4).
237 Moreover, ~ 150 m southward from the outcrop of the fault scarp, a 5×3 m wide trachyandesitic plug shows vertical
238 striation on its surface due to a subsurface vertical flow of the trachyandesite (Fig. 6e). The observed displacement at
239 the outcrop scale, as indicated by the height of the fault scarp, is ~ 10 m.

240 **4.1.4 Loma Blanca (LH-01, LH-02)**

241 The Loma Blanca Fault system (sites LH-01 and LH-02) is located in an active degassing area, where faults and
242 fractures are frequent. The fault system is on top of an elongated crest (within an apical depression) of a morphological
243 bulge, ~ 1 km in width and 30 m in height. At this location, the Cuicuiltic Member and the underlying trachyandesite
244 lavas are strongly altered (Fig. 6f). Evidence of stockwork veining and diffuse fracturing of the lavas suggests
245 hydrofracturing and structurally controlled fluid flow and alteration. A set of NNE-SSW striking conjugate extensional
246 faulting and jointing (joint spacing ~ 0.5 m) is observed. The faults (mean attitude $N26^{\circ}/71^{\circ}$, $n=6$) show normal dip-slip
247 kinematics (pitch of the slickenlines ranging 82° - 104°). Joint systems found in the Cuicuiltic Member strike sub-parallel
248 to the faults (mean attitude $N37^{\circ}/72^{\circ}$, $n=14$). The inferred cumulative displacement of the faults, estimated by the depth
249 of the apical depression, is ~ 5 m.

250 In summary, the 22 mapped faults in all the structural outcrops of the area show a main NNW-SSE strike (Fig. 6g) with
251 a dominant dip slip movement (mean pitch angle of slickenlines 88° , $n=16$) which is sub-parallel to the N-S elongation
252 of the lava domes and the Xalapasco crater.

253 **4.2 Experimental results**

254 Here we show three representative experiments with increasing overburden thickness (experiments 1-3-5 with $T=10$,
255 30 and 50 mm). Table 4 shows the measured parameters in the experiments. Some experiments (1-2 and 3-4) were
256 replicated with the same imposed boundary conditions and show the same result (i.e. apical depression width and dome
257 diameter), which ensures model reproducibility (Fig. 8 and Fig. S1).

258 Overall, the experiments show a similar deformation pattern: a first stage characterized by the uplift of a sub-circular
259 dome, bordered by inward dipping reverse faults, and a second stage characterized by the subsidence of the apical part
260 of the dome where normal faulting occurs (apical depression formation Fig. 7a-i). The reverse and normal faults are ring
261 faults and are associated with the formation of radial fractures from the dome centre. A different shape of the apical
262 depression is observed with $T/D > 0.12$. In exp.1 ($T/D = 0.12$) an annular peripheral depression formed as the silicone
263 reached the surface at the edge of the cylinder (Fig. 7c). Conversely, in exp. 3 and 5 ($T/D = 0.37$ and 0.63 respectively) a
264 sub-circular apical depression formed as the silicone reached the surface at the centre of the dome (Fig. 7g, m).

265 Irrespective of the T/D ratio, all experiments show that both the dome diameter and apical depression width increase
266 linearly with the overburden thickness (ranging from 105 to 164 mm and 14 to 58 mm respectively, Table 4, Fig. 8). The
267 dome diameter increases abruptly with time, becoming almost constant at an early stage of the experiment (Fig. 9a); the
268 apical depression width shows a similar pattern even if it enlarges slightly with time (after the first abrupt increase) as
269 the silicone rises towards the surface (Fig. 9b), suggesting that the intrusion depth has a higher influence on the apical
270 depression width, in agreement with Brothelande and Merle (2015).

271

272 **5. Discussion**

273 **5.1 Interpretation of the analogue experiments**

274 The deformation pattern observed in the analogue experiments for thicker overburdens (experiments 3-4 and 5 with
275 $T/D= 0.37$ and 0.63), showing a sub-circular dome and an apical depression, is in agreement with previous analogue
276 experimental results (Acocella et al., 2001; Marti et al. 1994; Walter and Troll 2001). However, for thinner overburdens
277 (exps. 1-2, $T/D= 0.12$), we observed a new deformation pattern at the surface consisting of an annular peripheral
278 depression due to the rising of the silicone at the edge of the cylinder rather than its centre. We infer that in these
279 experiments, since the rising silicone was very close to the surface, the sagging of the sand overburden pushed
280 downward the silicone that, consequently, squeezed up at the edges of the cylinder. Such process may also explain the
281 two linear grabens that formed in the experiments with elliptical sources for small overburden thicknesses (ratio $T/D \sim$
282 0.1 , Brothelande and Merle 2015).

283 The deformation pattern observed in our experiments is independent of the imposed strain (i.e. uplift) rate or the
284 viscosity of the intruding material as suggested by the similarity with results obtained in previous studies with higher
285 strain rates (Acocella and Mulugeta, 2002) or lower viscosity intruding materials (Galletto et al., 2017; Marti et al. 1994;
286 Walter and Troll, 2001). On the other hand, the occurrence of an apical depression is dependent on the thickness (i.e.
287 depth) of the intrusion since thin intrusions relative to their depths will generate sub-circular domes without any apical
288 depression (Galland et al., 2009; Galland, 2012). Moreover, our results confirm that the apical depression width shows a
289 linear correlation with the source depth (Fig. 8) as estimated in Brothelande and Merle (2015) for elongated sources.
290 This evidence documents that such relation is independent of the source eccentricity or shape of the extensional
291 structures at the top of the dome (i.e. linear graben or sub-circular depression) suggesting that any elongation of the
292 surface structure represents only a minor complication of the basic deformation pattern as already pointed out by
293 (Roche et al., 2000).

294

295 **5.2 Origin and extent of the resurgence in the LHVC**

296 The distribution of alteration patterns and deformation characteristics of the post-caldera deposits can be used to infer
297 the origin and extent of the uplift within the Los Potreros resurgent caldera. In particular, we focus on the Holocene
298 Cuicuiltic Member, which blankets the caldera floor.. Unaltered and undeformed deposits of the Cuicuiltic Member
299 crop out along the E-W Las Papas lineament and unconformably cover altered and faulted lavas and ignimbrites along
300 the Arroyo Grande and Maxtaloya scarps. Alteration and deformation of the Cuicuiltic Member occur along the Los
301 Humeros Fault scarp and within the apical depression of the Loma Blanca bulge. The vertical striations of the
302 trachyandesitic plug near the Los Humeros fault scarp suggest that the ascent of the plug induced the uplift, the normal
303 dip-slip faulting and alteration of the Cuicuiltic Member.

304 The observations suggest that Los Potreros is not a classic resurgent caldera (i.e. a caldera characterised by a large-scale
305 process localized in a single area) but is characterised by uplift pulses discontinuous in space and time, inducing small-
306 scale deformations at each pulse (Fig. 10a-d). In particular, it was active in the south and north-eastern sector of the
307 caldera, at Maxtaloya and Arroyo Grande (Fig. 10a), prior to the deposition of the Cuicuiltic Member (~ 7.4 ka), and
308 then shifted towards N along the Los Humeros and Loma Blanca scarps during and post the eruption of the Cuicuiltic
309 Member (Fig. 10b-d). The felsic lava found at the Los Humeros Fault scarp shows a similar mineral assemblage to the
310 felsic domes located further south (Fig. 4); thus, the Los Humeros scarp may represent the final stage (i.e. effusive
311 eruption of felsic magmas, Fig. 10c) of the uplift process, which is thus driven by the ascent of relatively narrow
312 (hundreds of meters) and highly viscous felsic magma batches. This is supported by the N-S elongation of the identified

313 lava domes which is sub-parallel to the orientation of the measured fault planes (NNW-SSE), indicating that the
314 observed deformation is closely related to the post-caldera volcanism. The emplacement of such magma bodies is
315 inferred here to drive the recent uplift and deformation of the Loma Blanca bulge, as suggested by the active fumaroles
316 and extensive alteration of both the Cuicuiltic Member and post-caldera lavas (Fig. 10d). The recent emplacement of
317 shallow magma bodies should be considered as a possible scenario for the interpretation of the seismicity in Los
318 Potreros, which have been so far interpreted as induced by geothermal exploitation (Lermo et al., 2018). In fact, the
319 highest magnitude of the recent seismicity reached between 3.2 and 4.2 and may well be consistent with a volcano-
320 tectonic origin due to shallow magma emplacement, more than induced by reinjection of hydrothermal fluids (cf. Evans
321 et al., 2012 and references therein).

322 To further support the above interpretation from field observations, results from the presented analogue models were
323 used to constrain the magma source depth from the geometrical parameters measured in the experiments (L_g , θ , α , Table
324 4). We calculated the theoretical overburden thickness (i.e. the intrusion depth, T_t , Table 4) as follow (Brothelande and
325 Merle, 2015):

$$326 \quad T_t = \frac{1}{2} L_g \times \frac{\sin(\theta + \alpha)}{\cos \theta} \quad (1)$$

327 Comparing the percentage difference (σ) between the imposed experimental (T) and theoretical (T_t) overburden
328 thickness values, we calculate the associated error in the evaluation of the intrusion depth in the models (σ , Table 4,
329 Fig.8). We then use equation (1) for the evaluation of the heat source depth at the Loma Blanca bulge considering $\sigma \sim$
330 40 % (maximum value of the experiments excluding those showing an annular depression that was not observed in the
331 field). For the Loma Blanca bulge $L_g = 286$ m, $\theta = 71^\circ$, $\alpha = 4.5^\circ$, the estimated intrusion depth is 425 ± 170 m. Such
332 relatively shallow depth is within the range of depths of rhyolitic-dacitic bodies drilled in geothermal wells (spanning
333 from -300 to -1700 m, Fig. 2a-b) and is consistent with the hypothesis that the uplift is driven by small and delocalized
334 magmatic intrusions, as suggested by the field data. These rhyolites-dacites bodies have been previously interpreted as
335 subaerial in origin (Carrasco-Núñez et al., 2017a), but we suggest that at least some of them can be reinterpreted as
336 intrusions of felsic cryptodomes based on the following considerations: (i) the occurrence of rhyolite-dacite lava bodies
337 within the thick pre-caldera old andesite sequence is unusual and does not have a subaerial counterpart; (ii) the rhyolite
338 body in well H-20 (Fig. 2b) up warps both the intracaldera ignimbrite sequence and the post-caldera lavas (showing a
339 reduced thickness) indicating that the caldera forming ignimbrites did not level out the paleo-topography, and (iii) the
340 top of the Xaltipan ignimbrite shows a higher depth variation than the pre caldera andesite (Fig. 2a) highlighting a local
341 and discontinuous uplifting of the Xaltipan ignimbrite. Such evidence can be more easily reconciled with the intrusion
342 of felsic cryptodomes within the volcanic sequence.

343

344 **5.3 Implications for the structure of the LHVC geothermal field**

345 The combination of field and modelling data support that the uplift in Los Potreros caldera is due to multiple
346 deformation sources in narrow areas that do not represent resurgence *sensu stricto*. Such localized recent deformation
347 within Los Potreros caldera appears to be linked to small magmatic intrusions located at relatively shallow depths (i.e. <
348 1 km) as in Loma Blanca, where the estimated intrusion depth calculated from the experimental data is 425 ± 170 m.

349 This model differs from the generally accepted idea of a resurgence in Los Potreros induced by the inflation of a saucer
350 or cup shaped deep magmatic intrusion (Norini et al., 2015, 2019), which may be active at a larger scale but does not
351 explain the highly discontinuous deformation and alteration patterns with pulses scattered along the caldera floor. Not
352 even the thermal anomalies identified by Norini et al. (2015) are compatible with the classic resurgence in Los Potreros,
353 since ground temperatures are unexpectedly cold beneath the centre of the inferred resurgent block, where the highest

354 temperatures should be instead expected. By contrast, sharp and narrow temperature peaks, spatially coincident with
355 Los Humeros and Loma Blanca faults, are consistent with the presence of shallow and delocalized heat sources. Indeed,
356 the inflation of the deep magma chamber of the LHVC, inferred to be at 5 to 7-8 km of depth (Verma, 1983, 2000,
357 2011) and extending 9 km in radius and 6 km in length (thus coinciding with the Los Humeros caldera rim, Verma et al.,
358 1990), should have induced a much wider uplift and with higher magnitude than the one observed in the field.
359 Resurgence resulting from magma remobilization of the deep chamber that produced collapse is characterized by a
360 larger-scale surface deformation (thousands of meters of uplift extending for tens of kilometres on the surface) as shown
361 in many large calderas worldwide (Toba, de Silva et al., 2015; Cerro Galan, Folkes et al., 2011; Ischia, Carlino, 2012,
362 Selva et al. 2019).

363 It is therefore unlikely that the replenishment of new magma in the caldera forming deep magma chamber accounts for
364 the magnitude (few tens of meters) and discontinuous spatial distribution of the deformation in Los Potreros.

365 Such a model of the recent uplifting in Los Potreros is supported by field-based petrographic-mineralogical analysis
366 showing that the present-day magmatic plumbing system is characterized by multiple magma levels spanning from a
367 deep (30-33 km) basaltic reservoir to very shallow (~ 1.5 km), smaller, trachyandesitic-trachytic magma batches (Lucci
368 et al., 2020).

369 A similar model of the plumbing system has been proposed to explain the eruptive activity of Usu volcano (Japan) since
370 1663, a post caldera cone of the Toya caldera consisting of a basaltic main edifice surmounted by three felsic lava
371 domes and more than ten cryptodomes. Petrochemical data at Usu suggest the presence of multiple magma batches (i.e.
372 sills) at 0.25-2 km deep that originated from partial melting of a metagabbro (Matsumoto and Nakagawa, 2010; Tomya
373 et al., 2010).

374 Our proposed model has implications for planning future geothermal exploration: siting of future geothermal wells
375 should consider that the presence of shallow heat sources within the caldera might complicate the pattern of isotherms
376 associated with the deeper heat flow.

377 **6 Conclusions**

378 By integrating field work with analogue models, we constrain the Late Pleistocene-Holocene spatio-temporal evolution
379 of volcanism of the LHVC and estimate the depth of the magmatic intrusions feeding the active geothermal system.
380 New findings on experimental analogue models of resurgent domes are also provided.

381 These are the main results that can be extracted from this study:

- 382 1. The distribution of the alteration patterns and deformation of the Cuicuiltic Member suggests that the recent (post-
383 caldera collapse) uplift in Los Potreros caldera moved progressively northwards, from the south and north-eastern
384 sector of the caldera towards N along the Los Humeros and Loma Blanca scarps.
- 385 2. The estimated depth of the intrusions responsible for such uplift is very shallow, as calculated from the experimental
386 data for the Loma Blanca bulge (425 ± 170 m).
- 387 3. The recent uplift in Los Potreros is discontinuous in space and time, inducing small-scale (areal extent ~ 1 km²)
388 deformations originating from multiple and shallow (< 1 km depth) magmatic bodies, thus not representing a classic
389 resurgent caldera, which usually involves large-scale deformation (areal extent of several km²).
- 390 4. The relationship between the depth of the magmatic source and the surface parameters of resurgent domes is
391 independent of the source eccentricity.

392

393 **Acknowledgements**

394 CFE is kindly acknowledged for allowing work on the Los Humeros geothermal field. Federico Galetto helped for laser
395 scanner data processing. Fabio Corbi and Matteo Trolese provided technical support in building the experimental set-up.
396 Gianluca Norini is acknowledged for logistic support in the field. Alessandra Pensa kindly helped with figure drawings.
397 Funded by the European Union's Horizon 2020 GEMex Project (grant agreement No. 727550) and by the Mexican
398 Energy Sustainability Fund CONACYT-SENER, WP 4.5 of the Project 2015-04-268074. More information can be
399 found on the GEMex Website: <http://www.gemex-h2020.eu>. The Grant to Department of Science, Roma Tre University
400 (MIUR-Italy Dipartimenti di Eccellenza, ARTICOLO 1, COMMI 314 – 337 LEGGE 232/2016) is gratefully
401 acknowledged.

402

403 **References**

404 Acocella, V.: Great challenges in volcanology: how does the volcano factory work?, *Front. Earth Sci.*, 2:4,
405 <https://doi.org/10.3389/feart.2014.00004>, 2014.

406 Acocella, V., and Funicello, R.: The interaction between regional and local tectonics during resurgent doming: the case
407 of the island of Ischia, Italy, *J. Volcanol. Geoth. Res.*, 88, 109-123, [https://doi.org/10.1016/S0377-0273\(98\)00109-7](https://doi.org/10.1016/S0377-0273(98)00109-7),
408 1999.

409 Acocella, V., and Mulugeta, G.: Experiments simulating surface deformation induced by pluton emplacement,
410 *Tectonophysics*, 352, 275-293, [https://doi.org/10.1016/S0040-1951\(02\)00218-4](https://doi.org/10.1016/S0040-1951(02)00218-4), 2002.

411 Acocella, V., Cifelli, F., and Funicello, R.: The control of overburden thickness on resurgent domes, *J. Volcanol. Geoth.*
412 *Res.*, 111, 137–153, [https://doi.org/10.1016/S0377-0273\(01\)00224-4](https://doi.org/10.1016/S0377-0273(01)00224-4), 2001.

413 Arellano, V.M., García, A., Barragán, R.M., Izquierdo, G., Aragón, A., and Nieva, D.: An updated conceptual model of
414 the Los Humeros geothermal reservoir (Mexico), *J. Volcanol. Geoth. Res.*, 124, 67–88, [https://doi.org/10.1016/S0377-
415 0273\(03\)00045-3](https://doi.org/10.1016/S0377-0273(03)00045-3), 2003.

416 Beavon, R.V.: A resurgent cauldron in the early Paleozoic of Wales, U.K., *J. Volcanol. Geoth. Res.*, 7, 157-174,
417 [https://doi.org/10.1016/0377-0273\(80\)90025-6](https://doi.org/10.1016/0377-0273(80)90025-6), 1980.

418 Brothelande, E., Peltier, A., Got, J.L., Merle, O., Lardy, M., and Garaebiti, E.: Constraints on the source of resurgent
419 doming inferred from analogue and numerical modeling — Implications on the current feeding system of the Yenkahe
420 dome–Yasur volcano complex (Vanuatu), *J. Volcanol. Geoth. Res.*, 322, 225–240,
421 <https://doi.org/10.1016/j.jvolgeores.2015.11.023>, 2016.

422 Brothelande, E., and Merle, O.: Estimation of magma depth for resurgent domes: An experimental approach, *Earth*
423 *Planet. Sc. Lett.*, 412, 143–151, <https://doi.org/10.1016/j.epsl.2014.12.011>, 2015.

424 Calcagno, P., Evanno, G., Trumpy, E., Carlos Gutiérrez-Negrín, L., Macías, J.L., Carrasco-Núñez, G., and Liotta, D.:
425 Preliminary 3-D geological models of Los Humeros and Acoculco geothermal fields (Mexico)-H2020 GEMex Project,
426 *Adv. Geosci.*, 45, 321–333, <https://doi.org/10.5194/adgeo-45-321-2018>, 2018.

427 Carlino, S.: The process of resurgence for Ischia Island (southern Italy) since 55 ka: The laccolith model and
428 implications for eruption forecasting, *B. Volcanol.*, 74, 947–961. <https://doi.org/10.1007/s00445-012-0578-0>, 2012.

429 Carrasco-Núñez, G., and Branney, M.J.: Progressive assembly of a massive layer of ignimbrite with a normal-to-reverse
430 compositional zoning: The Zaragoza ignimbrite of central Mexico, *B. Volcanol.*, 68, 3–20,
431 <https://doi.org/10.1007/s00445-005-0416-8>, 2005.

432 Carrasco-Núñez, G., McCurry, M., Branney, M.J., Norry, M., and Willcox, C.: Complex magma mixing, mingling, and
433 withdrawal associated with an intra-Plinian ignimbrite eruption at a large silicic caldera volcano: Los Humeros of
434 central Mexico, *Bull. Geol. Soc. Am.*, 124, 1793–1809, <https://doi.org/10.1130/B30501.1>, 2012.

435 Carrasco-Núñez, G., López-Martínez, M., Hernández, J., and Vargas, V.: Subsurface stratigraphy and its correlation
436 with the surficial geology at Los Humeros geothermal field, eastern Trans-Mexican Volcanic Belt, *Geothermics*, 67, 1–
437 17, <https://doi.org/10.1016/j.geothermics.2017.01.001>, 2017a.

438 Carrasco-Núñez, G., Hernández, J., De León, L., Dávila, P., Norini, G., Bernal, J.P., Jicha, B., Navarro, M., López-
439 Quiroz, P., and Digitalis, T.: Geologic Map of Los Humeros volcanic complex and geothermal field, eastern Trans-
440 Mexican Volcanic Belt, *Terra Digitalis*, 1, 1–11, <https://doi.org/10.22201/igg.terradigitalis.2017.2.24.78>, 2017b.

441 Carrasco-Núñez, G., Bernal, J.P., Dávila, P., Jicha, B., Giordano, G., and Hernández, J.: Reappraisal of Los Humeros
442 volcanic complex by new U/Th zircon and ⁴⁰Ar/³⁹Ar dating: Implications for greater geothermal potential, *Geochem.*
443 *Geophys. Geosy.*, 19, 132-149, <https://doi.org/10.1002/2017GC007044>, 2018.

444 Cashman, K. V., & Giordano, G.: Calderas and magma reservoirs, *J. Volcanol. Geoth. Res.*, 288, 28-45,
445 <https://doi.org/10.1016/j.jvolgeores.2014.09.007>, 2014.

446 Catalano, S., De Guidi, G., Lanzafame, G., Monaco, C., and Tortotici, L.: Late quaternary deformation on the island on
447 Pantelleria: new constraints for the recent tectonic evolution of the Sicily Channel Rift (southern Italy). *J. Geodyn.* 48,
448 75–82, 2009.

449 Chang, W.L., Smith, R.B., Wicks, C., Farrell, J.M., and Puskas, C.M.: Accelerated uplift and magmatic intrusion of the
450 Yellowstone Caldera, 2004 to 2006, *Science*, 318, 952-956, <https://doi.org/10.1126/science.1146842>, 2007.

451 Christiansen, R.L., Lipman, P.W., Carr, W.J., Byers, F.M., Orkild, P.P., and Sargent, K.A.: Timber Mountain-Oasis
452 Valley caldera complex of southern Nevada, *Geol. Soc. Am. Bull.*, 88, 943-959, [https://doi.org/10.1130/0016-7606\(1977\)88<943:TMVCCO>2.0.CO;2](https://doi.org/10.1130/0016-7606(1977)88<943:TMVCCO>2.0.CO;2), 1977.

454 Dávila-Harris, P., and Carrasco-Núñez, G.: An unusual syn-eruptive bimodal eruption: The Holocene Cuicuiltic
455 Member at Los Humeros caldera, Mexico, *J. Volcanol. Geoth. Res.*, 271, 24–42,
456 <https://doi.org/10.1016/j.jvolgeores.2013.11.020>, 2014.

457 de Silva, S.L., Mucek, A.E., Gregg, P.M., and Pratomo, I.: Resurgent Toba - field, chronologic, and model constraints
458 on time scales and mechanisms of resurgence at large calderas, *Front. Earth Sci.*, 3, 1–17,
459 <https://doi.org/10.3389/feart.2015.00025>, 2015.

460 Doblás, M.: Slickenside kinematic indicators, *Tectonophysics*, 295, 187–197, [https://doi.org/10.1016/S0040-1951\(98\)00120-6](https://doi.org/10.1016/S0040-1951(98)00120-6), 1998.

462 Du Bray, E.A., and Pallister, J.S.: Recrystallization and anatexis along the plutonic–volcanic contact of the Turkey
463 Creek caldera, Arizona, *Geol. Soc. Am. Bull.*, 111, 143–153, [https://doi.org/10.1130/0016-7606\(1999\)111<0143:RAAATP>2.3.CO;2](https://doi.org/10.1130/0016-7606(1999)111<0143:RAAATP>2.3.CO;2), 1999.

465 Elston, W.: Mid-Tertiary ash flow tuff cauldrons, southwestern New Mexico, *J. Geophys. Res.*, 89, 8733–8750,
466 <https://doi.org/10.1029/JB089iB10p08733>, 1984.

467 Evans, K.F., Zappone, A., Kraft, T., Deichmann, N., and Moia, F.: A survey of the induced seismic responses to fluid
468 injection in geothermal and CO₂ reservoirs in Europe, *Geothermics*, 41, 30-54,
469 <https://doi.org/10.1016/j.geothermics.2011.08.002>, 2012.

470 Ferrari, L., Orozco-Esquivel, T., Manea, V., and Manea, M.: The dynamic history of the Trans-Mexican Volcanic Belt
471 and the Mexico subduction zone, *Tectonophysics*, 522–523, 122–149, <https://doi.org/10.1016/j.tecto.2011.09.018>, 2012.

472 Ferriz, H., and Mahood, G.A.: Eruption Rates and Compositional Trends at Los Humeros Volcanic Center, Puebla,
473 Mexico, *J. Geophys. Res.*, 89, 8511-8524, <https://doi.org/10.1029/JB089iB10p08511>, 1984.

474 Folkes, C.B., Wright, H.M., R.A.F. Cas, de Silva, S.L., Lesti, C., and Viramonte, J.G.: A re-appraisal of the stratigraphy
475 and volcanology of the Cerro Galán volcanic system, NW Argentina, *B. Volcanol.*, 73, 1427–1454,
476 <https://doi.org/10.1007/s00445-011-0459-y>, 2011.

477 Fridrich, C.J., Smith, R.P., DeWitt, E., McKee, E.H.: Structural, eruptive, and intrusive evolution of the Grizzly Peak
478 caldera, Sawatch Range, Colorado, *Geol. Soc. Am. Bull.*, 103, 1160–1177, [https://doi.org/10.1130/0016-7606\(1991\)103<1160:SEAIEO>2.3.CO;2](https://doi.org/10.1130/0016-7606(1991)103<1160:SEAIEO>2.3.CO;2), 1991.

480 Galetto, F., Acocella, V., and Caricchi, L.: Caldera resurgence driven by magma viscosity contrasts, *Nat. Commun.*, 8,
481 1–11, <https://doi.org/10.1038/s41467-017-01632-y>, 2017.

482 Galetto, F., Bagnardi, M., Acocella, V., and Hooper, A.: Noneruptive unrest at the caldera of Alcedo Volcano (Galápagos
483 Islands) revealed by InSAR data and geodetic modelling, *J. Geophys. Res.*, 124, 3365–3381,
484 <https://doi.org/10.1029/2018JB017103>, 2019.

485 Galland, O.: Experimental modelling of ground deformation associated with shallow magma intrusions, *Earth Planet.
486 Sc. Lett.*, 317–318, 145–156, <https://doi.org/10.1016/j.epsl.2011.10.017>, 2012.

487 Galland, O., Planke, S., Ragnhild Neumann, E., and Malthe-Sørenssen, A.: Experimental modelling of shallow magma
488 emplacement: Application to saucer-shaped intrusions, *Earth Planet. Sc. Lett.*, 277, 373–383,
489 <https://doi.org/10.1016/j.epsl.2008.11.003>, 2009.

490 Giordano, G., Pinton, A., Cianfarra, P., Baez, W., Chiodi, A., Viramonte, J., Norini G., and GropPELLI, G.: Structural
491 control on geothermal circulation in the Cerro Tuzgle–Tocomar geothermal volcanic area (Puna plateau, Argentina), *J.
492 Volcanol. Geotherm. Res.*, 249, 77–94. <https://doi.org/10.1016/j.jvolgeores.2012.09.009>, 2013

493 Giordano, G., De Benedetti, A. A., Bonamico, A., Ramazzotti, P., and Mattei, M.: Incorporating surface indicators of
494 reservoir permeability into reservoir volume calculations: Application to the Colli Albani caldera and the Central Italy
495 Geothermal Province, *Earth-Sci. Rev.*, 128, 75–92, <https://doi.org/10.1016/j.earscirev.2013.10.010>, 2014.

496 Goto, Y., and McPhie, J.: Tectonics, structure, and resurgence of the largest Quaternary caldera in Japan: Kutcharo,
497 Hokkaido, *Geol. Soc. Am. Bull.*, 130, 1307–1322, <https://doi.org/10.1130/B31900.1>, 2018.

498 Guillou-Frottier, L., Burov, E.B., and Milési, J.P.: Genetic links between ash-flow calderas and associated ore deposits
499 as revealed by large-scale thermo-mechanical modelling, *J. Volcanol. Geoth. Res.*, 102, 339–361,
500 [https://doi.org/10.1016/S0377-0273\(00\)00246-8](https://doi.org/10.1016/S0377-0273(00)00246-8), 2000.

501 Hildreth, W., Fierstein, J., and Calvert, A.: Early postcaldera rhyolite and structural resurgence at Long Valley
502 Caldera, California, *J. Volcanol. Geoth. Res.*, 335, 1–34, <http://dx.doi.org/10.1016/j.jvolgeores.2017.01.005>, 2017.

503 Kennedy, B., Wilcock, J., and Stix, J.: Caldera resurgence during magma replenishment and rejuvenation at Valles and
504 Lake City calderas, *B. Volcanol.*, 74, 1833–1847, <https://doi.org/10.1007/s00445-012-0641-x>, 2012.

505 Kennedy, B., Holohan, E.P., Stix, J., Gravley, D.M., Davidson, J.R.J., and Cole, J.W.: Magma plumbing beneath
506 collapse caldera volcanic systems, *Earth-Sci. Rev.*, 177, 404–424, <https://doi.org/10.1016/j.earscirev.2017.12.002>, 2018.

507 Lipman, P. W.: The roots of ash flow calderas in Western North America: windows into the tops of granitic batholiths, *J.
508 Geophys. Res.*, 89, 8801–8841, <https://doi.org/10.1029/JB089iB10p08801>, 1984.

509 Lermo, J., Lorenzo, C., Jiménez, N., Ramos, E., Ângulo, J., Israel, J., Téllez, N., Machado, O., Álvarez, I., Torres, R.,
510 Alfaro R.: Analisis de la actividad sismica (1994-2016), su relacion con los pozos inyectoros y productores y aplicación
511 de nuevas tecnicas geofisica para caracterizar las zonas anómalas del campo geotérmico de Los Humeros, CEMIE-
512 GEO, Mexico, Internal Rep., 42 pp., 2018.

513 Lucci, F., Carrasco-Núñez, G., Rossetti, F., Theye, T., White, J. C., Urbani, S., Azizi, H., Asahara, Y., and Giordano, G.:
514 Anatomy of the magmatic plumbing system of Los Humeros Caldera (Mexico): implications for geothermal systems,
515 *Solid Earth Discuss.*, <https://doi.org/10.5194/se-2019-86>, 2020.

516 Marsh, B.D.: On the mechanics of caldera resurgence, *J. Geophys. Res.*, 89, 8245–8251,
517 <https://doi.org/10.1029/JB089iB10p08245>, 1984.

518 Martí, J., Ablay, G.J., Redshaw, L.T., and Sparks, R.S.J.: Experimental studies of collapse calderas, *J. Geol. Soc.*
519 *London*, 151, 919–929, <https://doi.org/10.1144/gsjgs.151.6.0919>, 1994.

520 Merle, O., Borgia, A.: Scaled experiments of volcanic spreading, *J. Geophys. Res.*, 101, 13805–13817,
521 <https://doi.org/10.1029/95JB03736>, 1996.

522 Morán-Zenteno, D.J., Alba-Aldave, L.A., Solé, J., and Iriondo, A.: A major resurgent caldera in southern Mexico: the
523 source of the late Eocene Tilzapotla ignimbrite. *J. Volcanol. Geoth. Res.*, 136, 97–119,
524 <https://doi.org/10.1016/j.jvolgeores.2004.04.002>, 2004.

525 Moretti, R., Troise, C., Sarno, F., and De Natale, G.: Caldera unrest driven by CO₂ induced drying of the deep
526 hydrothermal system, *Sci. Rep. UK*, 8, <https://doi.org/10.1038/s41598-018-26610-2>, 2018.

527 Mueller, W.U., Stix, J., Corcoran, P.L., Daigneault, R.: Subaqueous calderas in the Archean Abitibi greenstone belt: An
528 overview and new ideas, *Ore Geol. Rev.*, 35, 4–46, <https://doi.org/10.1016/j.oregeorev.2008.12.003>, 2009.

529 Norini, G., Groppelli, G., Sulpizio, R., Carrasco-Núñez, G., Dávila-Harris, P., Pelliccioli, C., Zucca, F., and De Franco,
530 R.: Structural analysis and thermal remote sensing of the Los Humeros Volcanic Complex: Implications for volcano
531 structure and geothermal exploration, *J. Volcanol. Geoth. Res.*, 301, 221–237,
532 <https://doi.org/10.1016/j.jvolgeores.2015.05.014>, 2015.

533 Norini, G., Carrasco-Núñez, G., Corbo-Camargo, F., Lermo, J., Hernández Rojas, J., Castro, C., Bonini, M., Montanari,
534 D., Corti, G., Moratti, G., Chavez, G., Ramirez, M., and Cedillo F.: The structural architecture of the Los Humeros
535 volcanic complex and geothermal field, *J. Volcanol. Geoth. Res.*, 381, 312–329.
536 <https://doi.org/10.1016/j.jvolgeores.2019.06.010>, 2019.

537 Matsumoto, A., and Nakagawa, M.: Formation and evolution of silicic magma plumbing system: Petrology of the
538 volcanic rocks of Usu volcano, Hokkaido, Japan, *J. Volcanol. Geoth. Res.*, 196, 185–207,
539 <https://doi.org/10.1016/j.jvolgeores.2010.07.014>, 2010.

540 Pribnow, D.F.C., Schütze, C., Hurter, S.J., Flechsig, C., Sass, J.H.: Fluid flow in the resurgent dome of Long Valley
541 Caldera: Implications from thermal data and deep electrical sounding. *J. Volcanol. Geoth. Res.*, 127, 329–345,
542 [https://doi.org/10.1016/S0377-0273\(03\)00175-6](https://doi.org/10.1016/S0377-0273(03)00175-6), 2003.

543 Roche, O., Druitt, T.H., and Merle, O.: Experimental study of caldera formation, *J. Geophys. Res.*, 105,
544 <https://doi.org/10.1029/1999JB900298>, 395–416, 2000.

545 Selva, J., Acocella, V., Bisson, M., Caliro, S., Costa, A., Della Seta, M., P. De Martino, S. de Vita, C. Federico,
546 G. Giordano, S. Martino, and C. Cardaci.: Multiple natural hazards at volcanic islands: a review for the Ischia volcano
547 (Italy), *Journal of Applied Volcanology*, 8(1), 5., <https://doi.org/10.1186/s13617-019-0086-4>, 2019

548 Smith, R. L., and Bailey, R. A.: Resurgent cauldrons, *Geol. Soc. Am. Mem.*, 116, 613–662,
549 <https://doi.org/10.1130/MEM116>, 1968.

550 Stix, J., Kennedy, B., Hannington, M., Gibson, H., Fiske, R., Mueller, W., Franklin, J.: Caldera-forming processes and
551 the origin of submarine volcanogenic massive sulfide deposits, *Geology*, 31, 375–378, [https://doi.org/10.1130/0091-7613\(2003\)031<0375:CFPATO>2.0.CO;2](https://doi.org/10.1130/0091-7613(2003)031<0375:CFPATO>2.0.CO;2), 2003.

552

553 Swanson, E., and McDowell, F.: Geology and geochronology of the Tomochic caldera, Chihuahua, Mexico, *Geol. Soc.*
554 *Am. Bull.*, 96, 1477-1482, [https://doi.org/10.1130/0016-7606\(1985\)96<1477:GAGOTT>2.0.CO;2](https://doi.org/10.1130/0016-7606(1985)96<1477:GAGOTT>2.0.CO;2), 1985.

555 Tomiya, A., Takahashi, E., Furukawa, N., Suzuki, T.: Depth and evolution of a silicic magma chamber: Melting
556 experiments on a low-K rhyolite from Usu volcano, Japan, *J. Petrol.*, 51, 1333-1354,
557 <https://doi.org/10.1093/petrology/egg021>, 2010.

558 Ueda, H., Nagai, M., and Tanada, T.: Phreatic eruptions and deformation of Ioto Island (Iwo-jima), Japan, triggered by
559 deep magma injection, *Earth Planets Space*, 70, <https://doi.org/10.1186/s40623-018-0811-y>, 2018.

560 Verma, M.P., Verma, S.P., and Sanvicente, H.: Temperature field simulation with stratification model of magma
561 chamber under Los Humeros caldera, Puebla, Mexico, *Geothermics*, 19, 187-197, [https://doi.org/10.1016/0375-](https://doi.org/10.1016/0375-6505(90)90015-4)
562 [6505\(90\)90015-4](https://doi.org/10.1016/0375-6505(90)90015-4), 1990.

563 Verma, S.P., Gómez-Arias, E., and Andaverde, J.: Thermal sensitivity analysis of emplacement of the magma chamber
564 in Los Humeros caldera, Puebla, Mexico, *Int. Geol. Rev.*, 53, 905-925, <https://doi.org/10.1080/00206810903234296>,
565 2011.

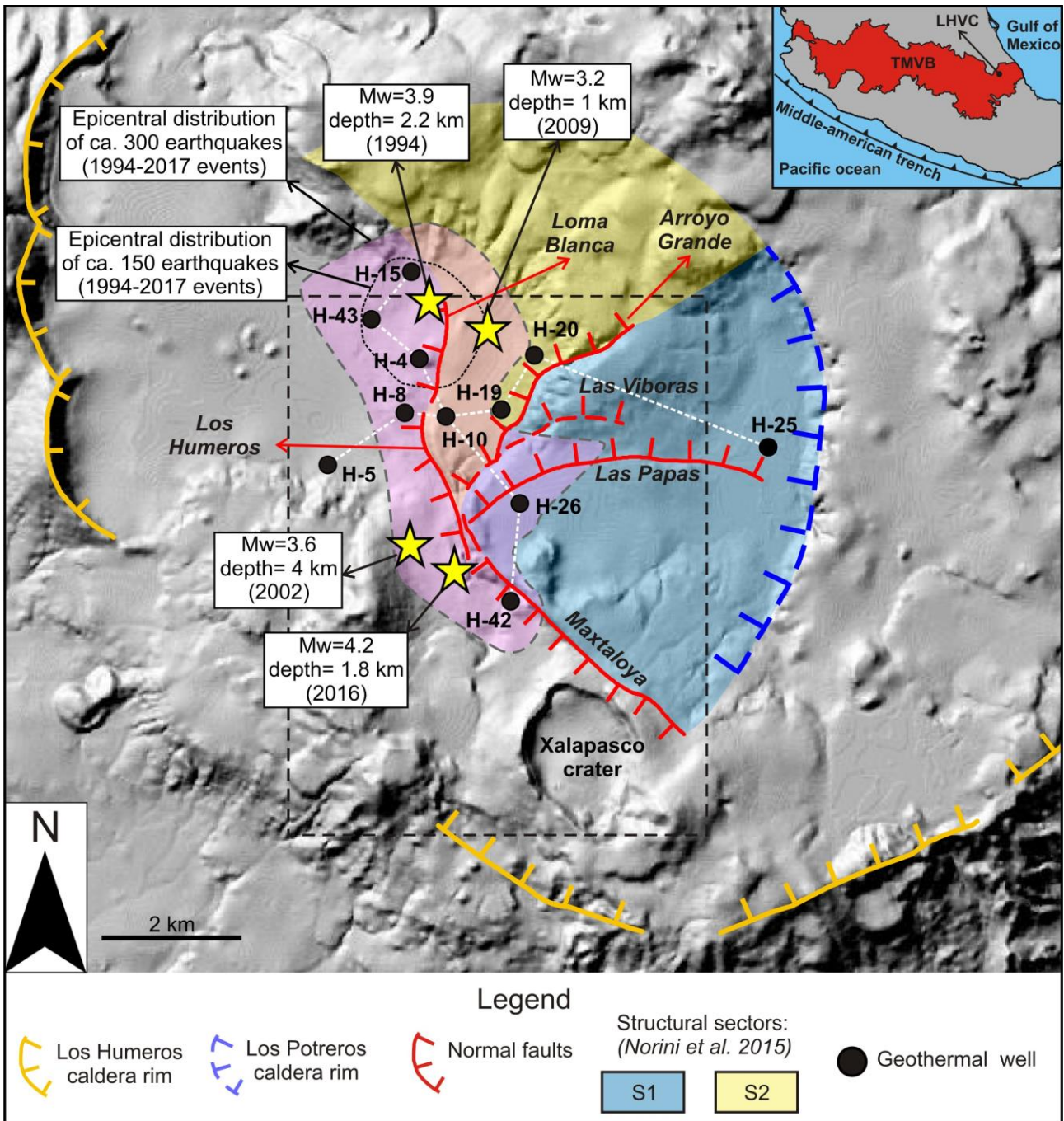
566 Verma, S.P.: Magma genesis and chamber processes at Los Humeros caldera, Mexico - Nd and Sr isotope data, *Nature*,
567 302, 52-55, <https://doi.org/10.1038/302052a0>, 1983.

568 Verma, S.P.: Geochemical evidence for a lithospheric source for magmas from Los Humeros caldera, Puebla, Mexico.
569 *Chem. Geol.* 164, 35-60, [https://doi.org/10.1016/S0009-2541\(99\)00138-2](https://doi.org/10.1016/S0009-2541(99)00138-2), 2000.

570 Vignaroli, G., Pinton, A., De Benedetti, A. A., Giordano, G., Rossetti, F., Soligo, M., and Berardi, G.: Structural
571 compartmentalisation of a geothermal system, the Torre Alfina field (central Italy), *Tectonophysics*, 608, 482-498.
572 <https://doi.org/10.1016/j.tecto.2013.08.040>, 2013. Vignaroli, G., Aldega, L., Balsamo, F., Billi, A., De Benedetti, A. A.,
573 De Filippis, L., Giordano G. and Rossetti, F.: A way to hydrothermal paroxysm, Colli Albani volcano, Italy, *Geol. Soc.*
574 *Am. Bull.*, 127(5-6), 672-687. <https://doi.org/10.1130/B31139.1>, 2015.

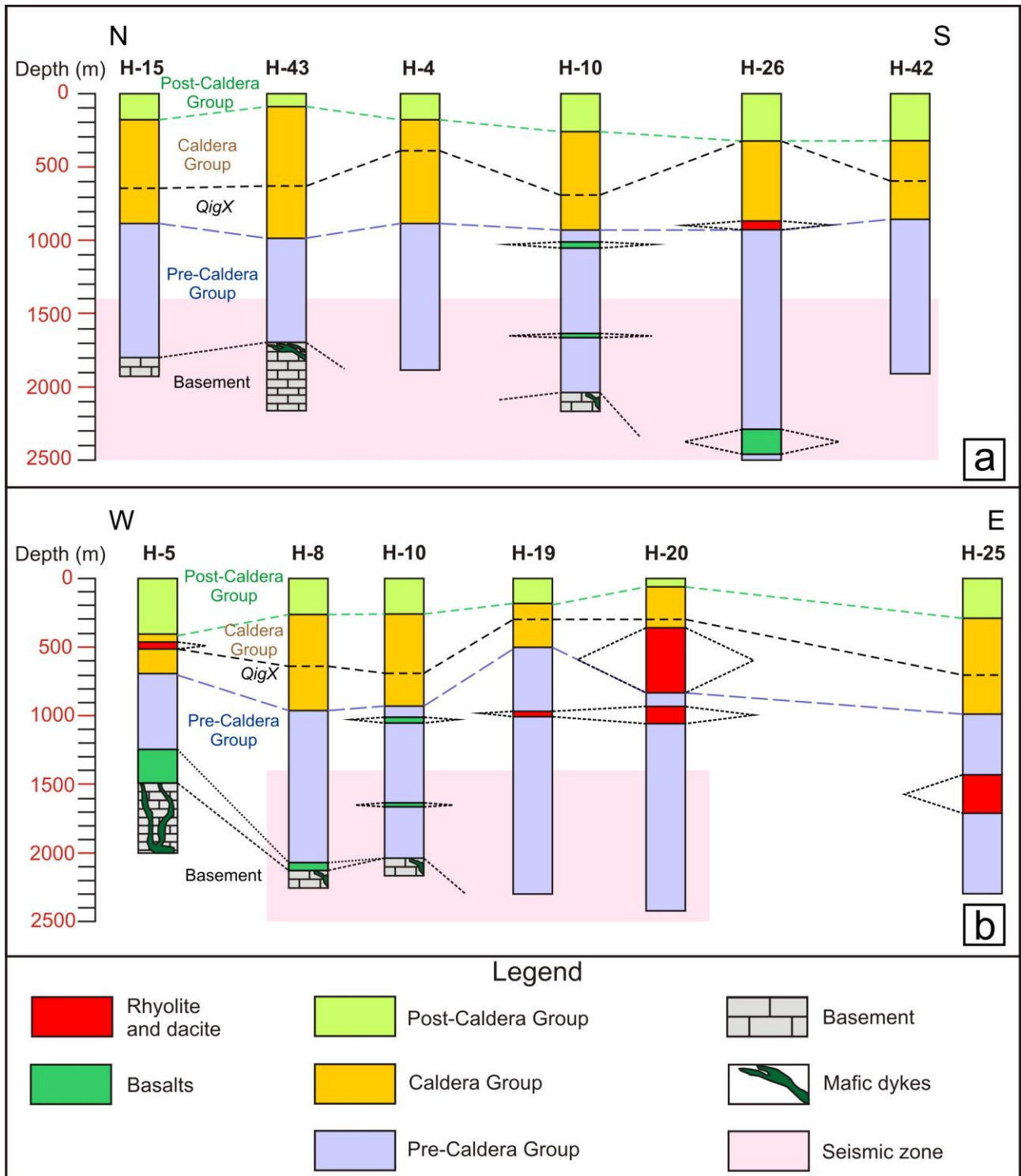
575 Walter, T.R., and Troll, V.R.: Formation of caldera periphery faults: an experimental study, *B. Volcanol.*, 63, 191-203,
576 <https://doi.org/10.1007/s004450100135>, 2001. Walter, T.R., Wang, R., Acocella, V., Neri, M., Grosser, H., and Zschau, J:
577 Simultaneous magma and gas eruptions at three volcanoes in southern Italy: an earthquake trigger ?, *Geology*, 37, 251-
578 254, <https://doi.org/10.1130/G25396A>, 2009.

579 Wilcox, C.P.: Eruptive, magmatic and structural evolution of a large explosive caldera volcano, Los Humeros, Central
580 Mexico, Ph.D. thesis, Department of Geology, University of Leicester, United Kingdom, 317 pp., 2011.



581
 582 **Figure 1:** Shaded relief image (illuminated from the NE) obtained from 15 m resolution DEM of the Los Humeros Volcanic
 583 Complex (LHVC) showing the main structural features (faults and caldera rim, modified from Norini et al. (2015); Calcagno
 584 et al. (2018) and some geothermal wells referred in the text and in Figures 2a-b. The white dashed lines indicate the direction
 585 of the correlation sections shown in Figures 2a-b. The black rectangle indicates the studied area within the Los Potreros
 586 Caldera shown in Figure 4. The Inset box show the location of the LHVC (black dot and arrow) within the eastern sector of
 587 the Trans Mexican Volcanic Belt (TMVB). The structural sectors S1 and S2 correspond to the resurgent block inferred by
 588 Norini et al. (2015). Seismicity data from Lermo et al. (2018).

589
 590
 591
 592
 593



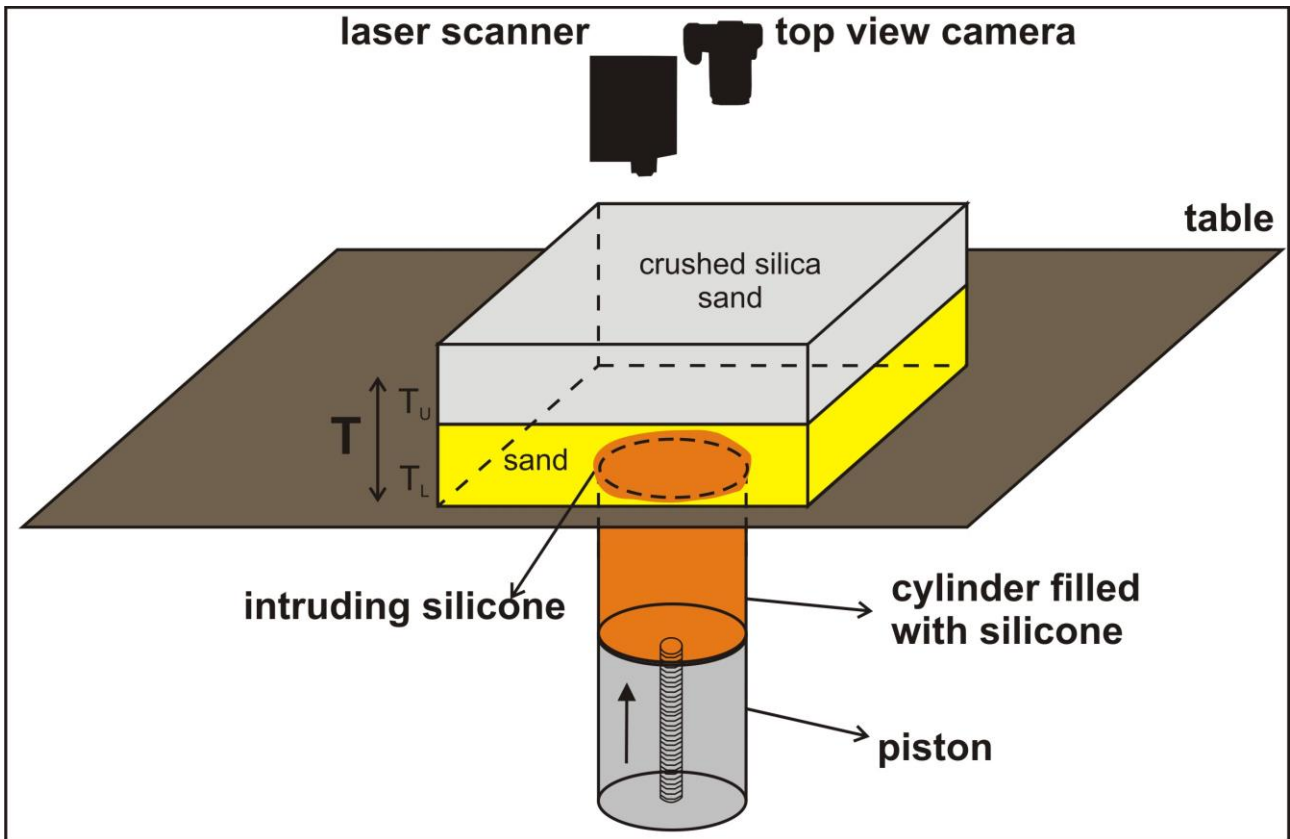
594

595

596

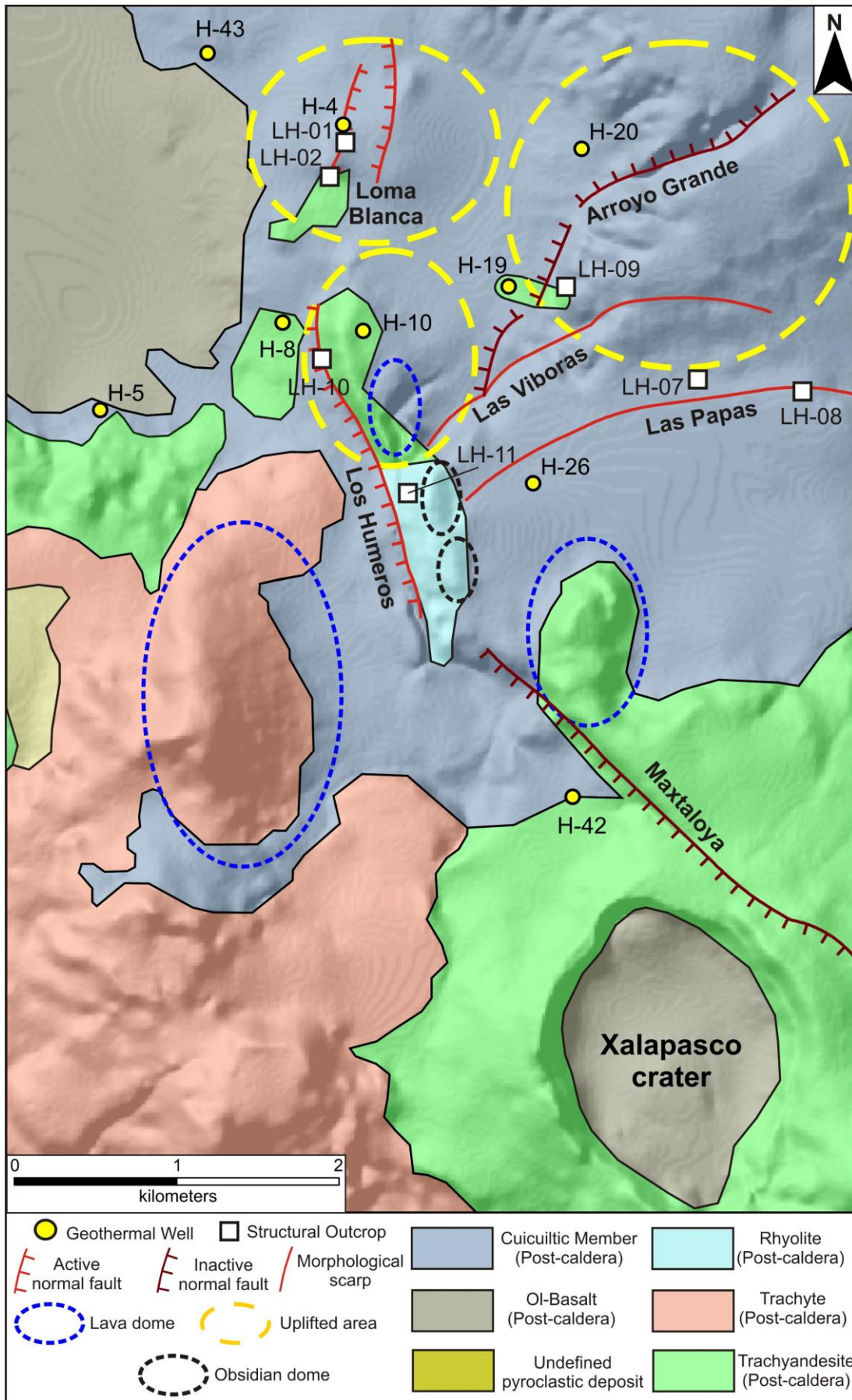
597

Figure 2: In depth correlation of lithostratigraphic units along the N-S (a) and W-E (b) direction (redrawn after Carrasco-Núñez et al. (2017a) and Arellano et al. (2003). Depth:horizontal distance=1:1. Location of the correlation line is shown in Figure 1. QigX= Xaltipan ignimbrite.



598
 599
 600
 601
 602
 603
 604
 605
 606
 607
 608
 609
 610
 611
 612
 613
 614
 615
 616
 617
 618
 619
 620
 621

Figure 3: Experimental set-up. A motor controlled piston pushes upward the silicone at a fixed rate (2mm/hr) from the base of the layered sand pack (the diameter of the silicone is 8 cm). A laser scanner and a camera record the surface deformation induced by the intruding silicone. T = total overburden thickness. T_U = upper layer thickness, T_L = lower layer thickness.

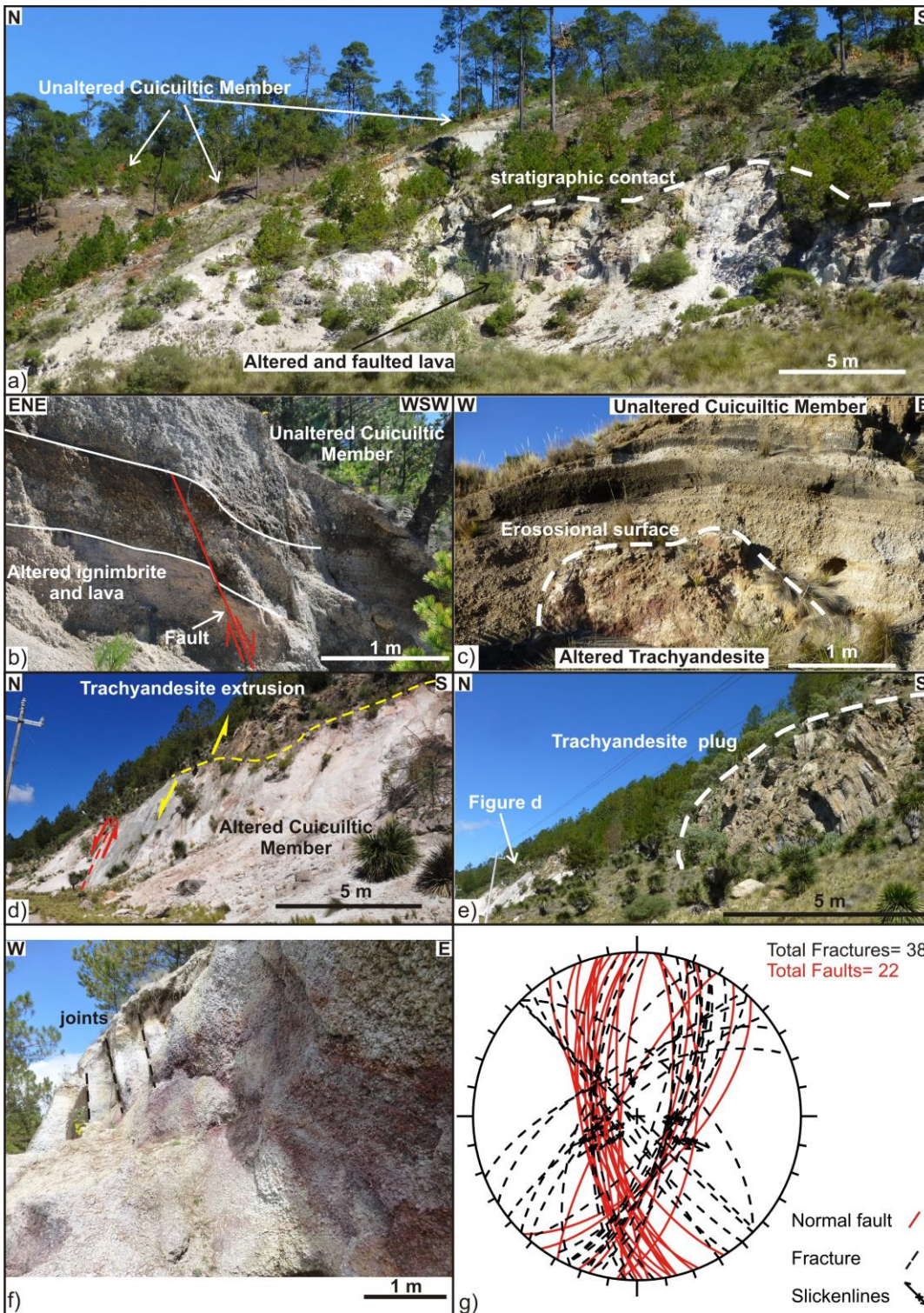


622
623
624

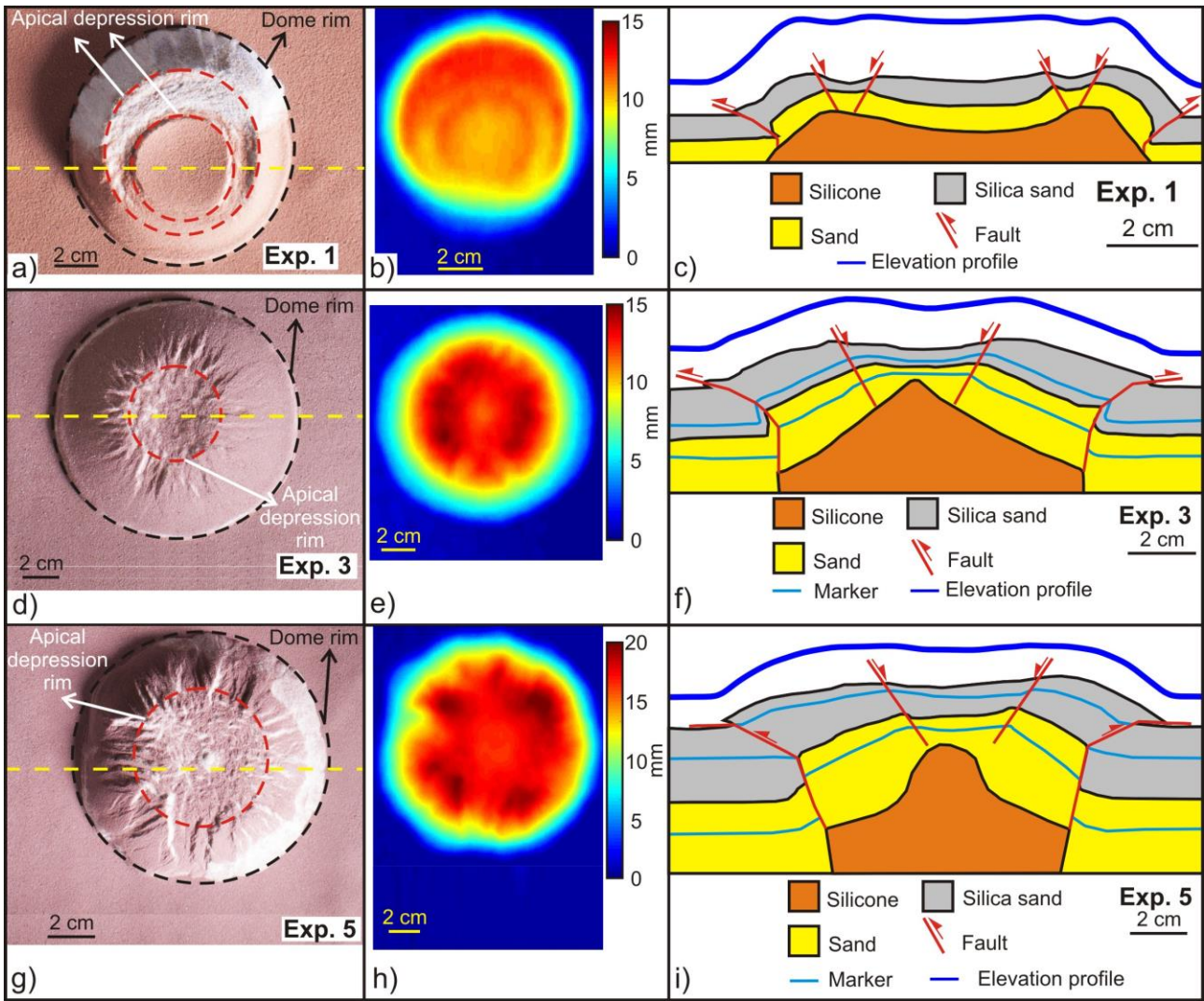
Figure 4: Simplified geological structural map of the studied area; reinterpreted after (Norini et al., 2015; Carrasco- Núñez et al., 2017b; Calcagno et al., 2018).



625
 626 **Figure 5: a) Panoramic view from Xalapasco crater (looking towards N) of the lava domes aligned N-S. b) Unaltered**
 627 **Cuicuiltic Member (LH-07). c) Unaltered Cuicuiltic Member covering a layered pyroclastic deposit, which can be laterally**
 628 **correlated with the Xoxoctic Tuff (LH-08). The erosional surface preceding the deposition of the Cuicuiltic Member is shown**
 629 **(dashed white line).**

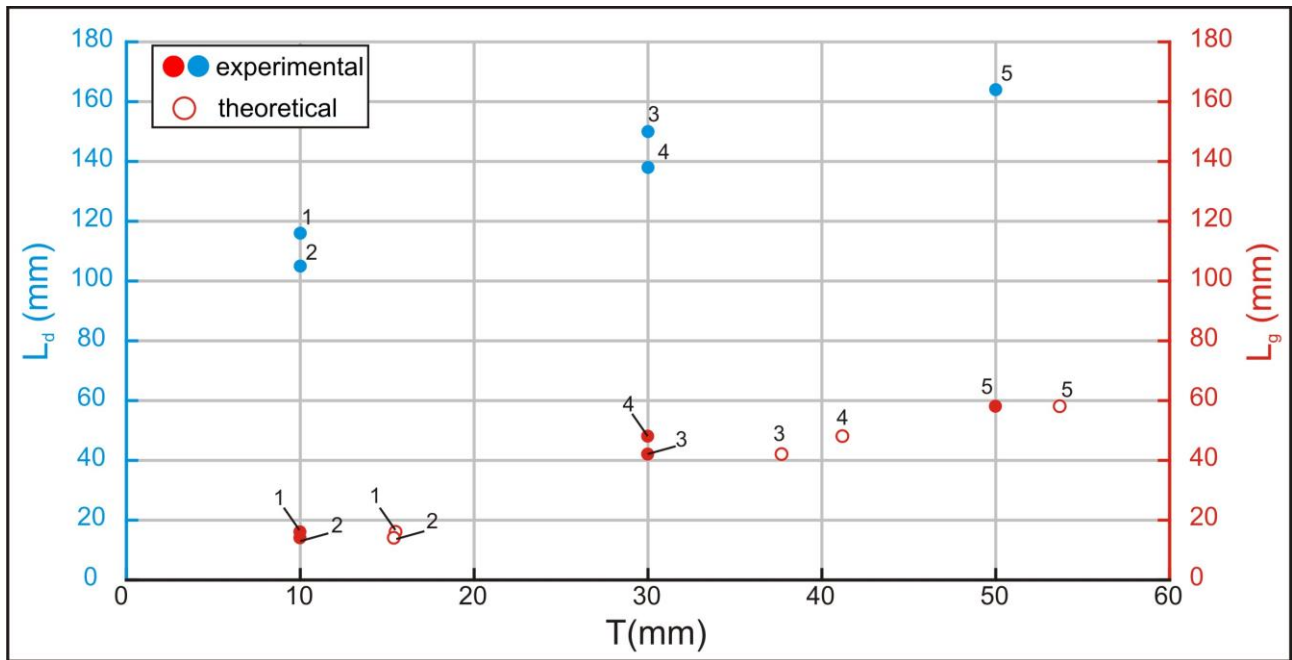


630
 631 **Figure 6:** a) Panoramic view of the Arroyo Grande fault scarp showing the unaltered Cuicuiltic Member covering the altered
 632 and faulted ignimbrite and lavas (site LH-09). b) Normal fault affecting the altered ignimbrite deposits unconformably
 633 covered by the post-caldera, unaltered Cuicuiltic Member deposits (LH-09). Note that the Cuicuiltic Member deposits are
 634 not faulted at this location; the fault can be thus considered as a fossil fault with respect to the Cuicuiltic Member deposition.
 635 c) Block of altered trachyandesite buried by unaltered Cuicuiltic Member layers along the Maxtaloya fault scarp. d) Los
 636 Humeros fault scarp (LH-10) induced by the ascent of the trachyandesitic extrusion on top of the fault plane. e)
 637 Trachyandesite plug cropping out ~150 southward the fault scarp shown in d) (indicated by the red arrow). f) Jointing and
 638 alteration of the Cuicuiltic Member within the apical depression of the Loma Blanca dome (LH-01). e) Equal-area stereo-plot
 639 of the attitudes of faults and fractures in all the structural outcrops.



640
641
642
643
644
645
646
647
648
649
650
651
652
653
654
655
656
657
658

Figure 7: a) d) g) Top view image of the experiments 1, 3 and 5. b) e) h) cumulative vertical displacement; colour scale is proportional to the amount of uplift. c) f) i) Drawing of the cross section view obtained after cutting the section close to the dome center. The elevation profiles are obtained from laser scanner data. The yellow dashed line in a) d) g) indicates the trace of the section views and of the elevation profiles.

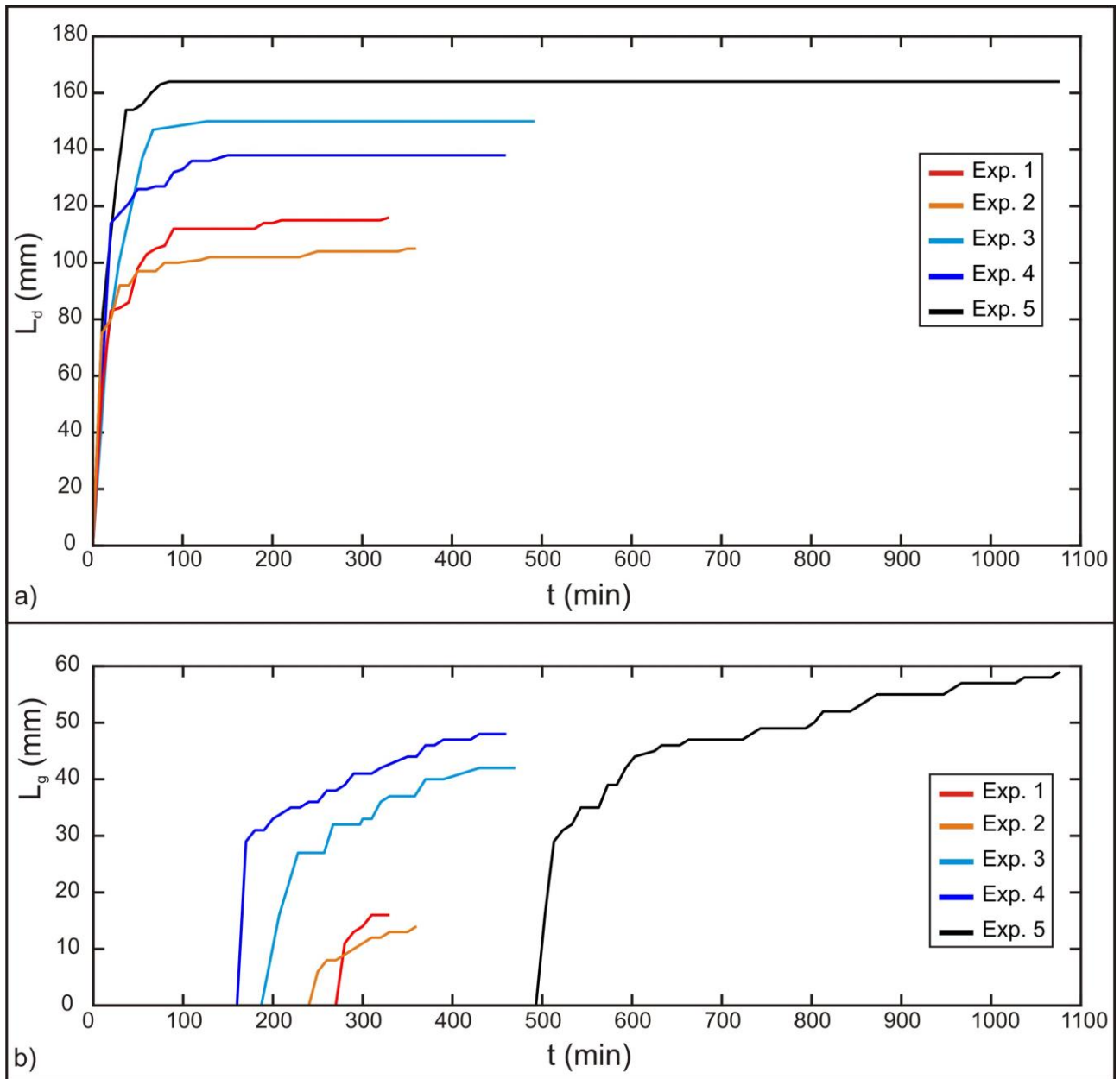


659

660

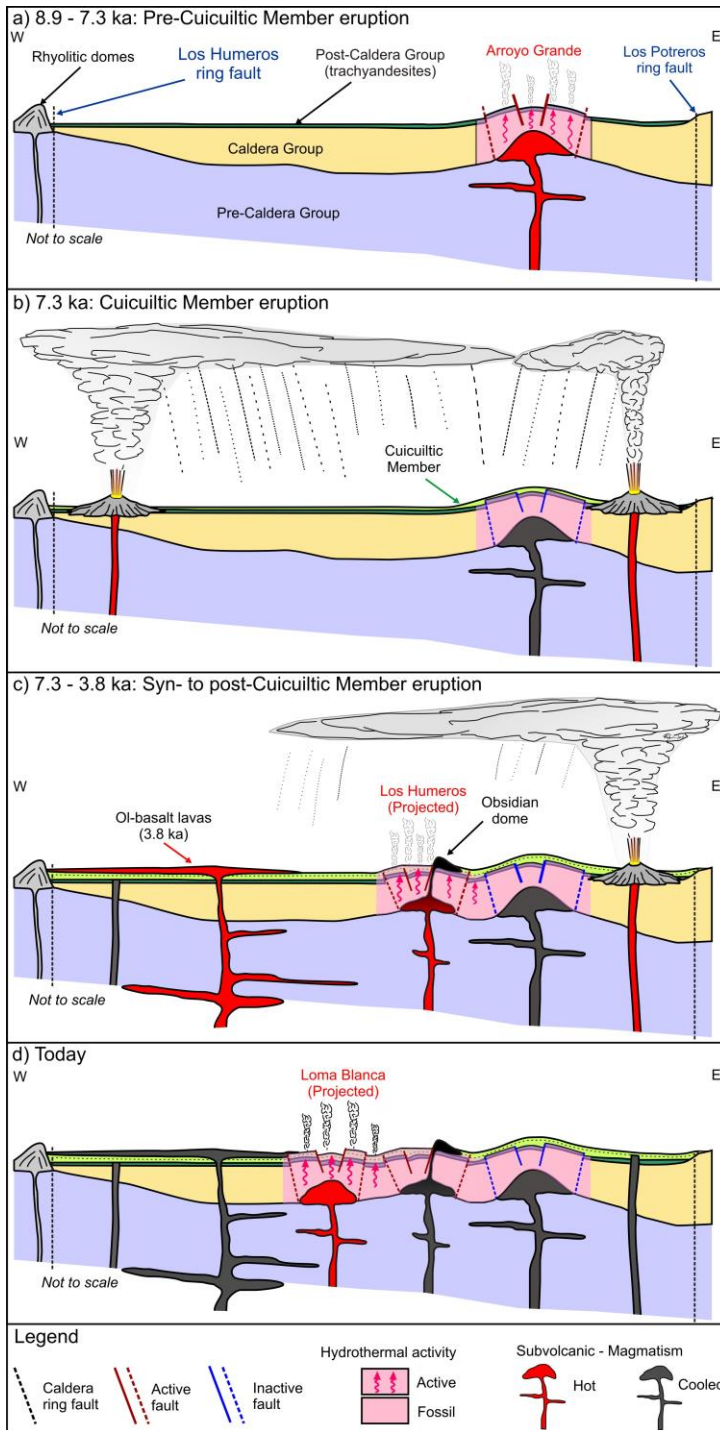
661

Figure 8: L_g (apical depression width) and L_d (dome diameter) versus T (overburden thickness). Theoretical values calculated after equation 1 (see discussion section). The numbers above each point indicate the experiment number.



662
 663 **Figure 9: a) Time evolution of the dome diameter (L_d). b) Time evolution of the apical depression width (L_g). Both L_d and L_g**
 664 **show a similar evolution trend with a first stage of abrupt increase at the beginning of each experiment. In the second stage**
 665 **L_d becomes constant at $t \sim 90$ min (experiments 1-2-3), $t \sim 150$ min (experiment 4) and $t \sim 65$ min (experiment 5) while L_g**
 666 **increases slightly from $t \sim 250$ -280 min (experiments 1-2), $t \sim 210$ min and ~ 170 min (experiments 3 and 4) and $t \sim 530$ min**
 667 **(experiment 5) till the end of the experiment.**

668
 669
 670
 671
 672
 673
 674
 675
 676
 677



678

679

680

681

682

683

684

685

686

687

688

689

Figure 10: Schematic model of the evolution of the sub-surface structure of the Los Potreros caldera floor. Multiple magmatic intrusions located at relatively shallow depth (< 1 km) are responsible for the localized bulging of the caldera floor (Loma Blanca, Los Humeros and Arroyo Grande uplifted areas). a) Pre Cuicuiltic Member eruption: emplacement of a felsic intrusion at shallow depth and formation of the Arroyo grande bulge characterized by extensional faulting at its top, reverse faulting at its base and hydrothermalism. b) Cuicuiltic Member eruption: eruption of the Cuicuiltic Member covering the hydrothermally altered post-caldera trachyandesitic lavas. c) Syn to post Cuicuiltic Member eruption: formation of the Los Humeros fault and extrusion of obsidian lava domes along the fault scarp. As the trachyandesitic domes are covered with Cuicuiltic Member only at his base, the lava extrusion occurred during and post the Cuicuiltic Member eruption. d) Formation of the Loma Blanca bulge with the current hydrothermal activity and extensional faulting occurring within the apical depression. Notice that the emplacement of the successive most recent domes (Los Humeros and Loma blanca) are not aligned on the same plane, they are shown for practical purposes.

Stage	Age (ka)	Main stratigraphic units
Post-caldera	< 69	Cuicuiltic Member and trachyandesitic to basaltic lavas
		Llano Tuff
		Xoxoctic Tuff
		Rhyolitic domes
Caldera	164-69	Zaragoza ignimbrite
		Faby Tuff
		Xaltipan ignimbrite
Pre-Caldera	700-164	Rhyolitic Domes

690 Table 1 Summary of the main stratigraphic units of the three evolutionary stages of the Los Humeros Volcanic complex
691 (Carrasco-Núñez et al., 2017b, 2018).

Parameter	Definition	Value (experiments)	Value (nature)
T	Thickness of the overburden	1-5 X 10 ⁻² m	300-2000 m
L _d	Dome diameter	1-1.6 X 10 ⁻¹ m	2000 m
H	Dome height	1.1-2 X 10 ⁻² m	100 m
ρ _s	Density of brittle overburden	1400 kg/m ³	2800 kg/m ³
φ	Angle of internal friction	35°	25-40°
τ ₀	Cohesion (brittle overburden)	300 Pa	10 ⁶ Pa
ρ _m	Density of intrusive material	1000 kg/m ³	2500 kg/m ³
μ _m	Viscosity of intrusive material	10 ⁴ Pa s	10 ¹⁵ Pa s
g	Gravity	9.8 m/s ²	9.8 m/s ²
t	Timespan for deformation	2.8-6.5 X 10 ⁴ s	1.9 X 10 ¹² s

692 Table 2. Comparison of the geometric and material properties parameters of the experiments and nature.

Dimensionless ratio	Experiments	Nature
Π ₁ = T/L _d	0.1-0.5	0.15-1
Π ₂ = H/L _d	0.08-0.2	0.05-0.1
Π ₃ = ρ _s /ρ _m	1.4	1.12
Π ₄ = φ	35	25-40
Π ₅ = ρ _m H ² /μ _{mt}	6.1 X 10 ⁻¹⁰	1.3 X 10 ⁻²⁰
Π ₆ = ρ _m gHt/μ _m	1.3 X 10 ³	4.6 X 10 ³
Π ₇ = ρ _s gT/τ ₀	2.3	8.24

693 Table 3. Definition and values of the dimensionless ratios Π in nature and in the experiments.

Exp	T (mm)	L _g (mm)	L _d (mm)	θ	α	T _t (mm)	σ (%)
1	10	16	116	58°	14°	15.5	55
2	10	14	105	63°	27°	15.4	54
3	30	42	150	58°	14°	37.7	27
4	30	48	138	56°	18°	41.2	37
5	50	58	164	58°	21°	53.7	7

694 Table 4. Measured (L_g, L_d, θ, α) and imposed (T) parameters in the experiments. T=overburden thickness; L_d= dome
695 diameter; L_g= apical depression width; θ= apical depression fault dip; α= dome flank mean dip; T_t= theoretical overburden

696 thickness calculated with equation 1 (Brothelände and Merle, 2015, see discussion section); σ = percentage difference between
697 T and T_c .